FLIPs: Novel Genetically Encoded Biosensors for Functional Imaging of Cell Signaling by Polarization Microscopy

Paul Miclea, Vendula Nagy-Marková, Alina Sakhi, Alexey Bondar, Josef Lazar

Abstract

Genetically encoded fluorescent biosensors convert specific biomolecular events into optically detectable signals. By revealing biochemical processes *in situ*, they have revolutionized cell biology. However, imaging molecular processes often requires modifying the proteins involved, and many molecular processes are still to be imaged. Here we present a novel, widely applicable design of genetically encoded biosensors that notably expand the observation possibilities, by taking advantage of a hitherto overlooked detection principle: directionality of optical properties of fluorescent proteins. The probes, which we term FLIPs, offer an extremely simple design, high sensitivity, multiplexing capability, ratiometric readout and resilience to bleaching artifacts, without requiring any modifications to the probe targets. We demonstrate their performance on real-time single-cell imaging of activation of G protein-coupled receptors (GPCRs), G proteins, arrestins, small GTPases, as well as receptor tyrosine kinases, even at endogenous expression levels. We also identify a new, pronounced, endocytosis-associated conformational change in a GPCR–β-arrestin complex. By demonstrating a novel detection principle and allowing many more cellular processes to be visualized, FLIPs are likely to inspire numerous future developments and insights.

Main

Genetically encoded fluorescent biosensors allow visualizing specific cellular processes in living cells, tissues and animals. Such probes are often constructed by fusing a sensing protein to a fluorescent moiety (such as a fluorescent protein (FP)), creating a causal connection between the molecular process of interest and the fluorescent output[1,2]. Usually, a conformational or structural change in the sensing protein is used to modulate one of several modes of fluorescence quenching, most often through facilitating (or restricting) access of water molecules to the fluorophore (e.g., in circularly permuted FPs), or through providing (or removing) a suitable excitation energy donor or acceptor (e.g., in bioluminiscence or fluorescence resonant energy transfer). The requirement for a sufficiently large conformational change in the sensing protein severely limits the number of phenomena that can be probed. Furthermore, many such biosensors require an insertion of a fluorescent moiety into the protein of interest (e.g. a receptor protein), leading to perturbations in its function. Although so-called translocation sensors, responding by redistribution of a fluorophore across the cell[3,4], avoid the need for a conformationally-switching protein, their responses are hard to quantify and the number of their targets is limited.

Thus, there remains a strong need for new biosensors that would allow real-time *in vivo* observations of functional activity of a wide range of non-modified, endogenously expressed proteins, providing quantifiable, ratiometric readout while allowing multiplexing. In order to try to meet this need, we decided to exploit the well documented, but seldom utilized effects of optical directionality of fluorescent proteins.

Briefly, fluorescent molecules (including fluorescent proteins) behave like dipole antennas, with distinctly directional properties[5,6]. The directionality is characterized by vectors: the transition dipole moments (TDMs). Molecules preferentially absorb light polarized parallel to their excitation TDM (xTDM). The direction and polarization of their fluorescence are determined by the orientation of an emission TDM (mTDM). Optical directionality manifests itself as differences in absorption of light of distinct linear polarizations (linear dichroism, LD), and as fluorescence polarization. The two phenomena can report on molecular orientation at the instant of light absorption and emission, respectively. However, despite its appealing qualities (intrinsically ratiometric readout, possibility of multiplexing due to the need for only a single spectral band, relative instrumental simplicity), optical directionality has so far found only a limited number of uses in microscopy[7-13]. The existing biosensors based on optical directionality modify the proteins of interest[14], their design is specific for each application, the observed responses are usually small[15], and efforts at improvements have largely been non-productive[8,15]. For optical directionality to become useful, these drawbacks would have to be overcome.

To address this challenge, we have now created a novel class of molecular probes that we term FLIPs (**F**luorescence anisotropy and **LI**near dichroism **P**robes) (Fig. 1a). Briefly, FLIPs consist of a fluorescent moiety (an FP) bearing at one of its termini a flexible linker and a membrane-targeting moiety, and at the other terminus a moiety capable of binding the target of the probe. In absence of the probe's target, the FP moiety is expected to adopt a largely random molecular orientation, while in presence of the target, the orientation of the FP with respect to the cell membrane becomes restricted. The differences in orientational distributions of the FP can be easily observed as changes in linear dichroism and fluorescence polarization.

Initial FLIP designs

To test the FLIP design (Fig. 1), we prepared several constructs based on the peptide KB1753 which binds the activated form of the G protein Gαi1[16,17]. The enhanced green fluorescent protein (eGFP) served as the fluorescent moiety. We used the hexapeptide Gly-Ser-Gly-Gly-Ser-Gly as the flexible linker. Finally, as membrane anchors[18] we tested the N-terminal palmitoylation signal peptide derived from GAP43, the transmembrane domain of the interleukin receptor IL4Rα, the C-terminal palmitoylation/farnesylation domain of H-Ras, and the C-terminal farnesylation domain of K-Ras.

To determine whether the four probes (GAP43-eGFP-KB1753, IL4R-eGFP-KB1753, KB1753-eGFP-HRas, KB1753-eGFP-KRas) interact with the intended target, we observed their linear dichroism of in living HEK293 cells, in absence and in presence of a constitutively active mutant of Gαi1 (Gαi1(Q204L)-IRES-mCherry or Gαi1(Q204L)-IRES-mTurquoise2; both denoted as Gαi1*). The results are illustrated in Fig 2, Suppl. Figs 1-3, and summarized in Table 1. With the exception of GAP43-eGFP-KB1753, we observed striking differences in LD between cells expressing only a probe and those co-expressing the probe and Gαi1*. The effect was most

pronounced in IL4Rα-eGFP-KB1753 which, however, showed irregular membrane localization. Thus, we selected KB1753-eGFP-HRas for further development and testing. Modifying the length of the flexible linker brought little benefit, as probes with longer linkers exhibited smaller changes in LD, and, ultimately, poorer cell membrane localization (Suppl. Fig. 3).

Replacing the eGFP moiety with other FPs (Fig 2c, d) affected the directional optical properties of the KB1753-FP-HRas constructs, often in unexpected ways. For example, KB1753-mTurq2-HRas showed pronounced LD in absence of Gαi1*, and almost no LD in presence of Gαi1*. Thus, constructs differing solely in a few amino acids of the FP moiety (eGFP and mTurquoise2 show 97% amino acid identity apart from the fluorophore) exhibited opposite Gαi1*-induced behaviors. KB1753-cpsfGFP-HRas, a FLIP containing a circularly permuted version of GFP[19], showed a behavior similar to that observed in KB1753-mTurq2-HRas (containing a non-permuted mTurquoise2[20]). Strikingly, KB1753-cpmTurq2-HRas, bearing a circularly permuted version of mTurquoise2, showed pronounced LD both in absence and in presence of Gαi1* - but with opposite signs. Finally, KB1753-mScarlet-HRas exhibited LD values similar to those of KB1753-eGFP-HRas, despite the sequences of eGFP and mScarlet being completely dissimilar. Without detailed investigations, we attribute the observed unexpected differences in behavior of similar constructs to sequence-specific interactions between the FP moiety and the plasma membrane. In the future, such interactions may be exploited in rational development of improved FLIPs.

Importantly, our results demonstrate that FLIPs can accommodate a wide range of FPs spanning the whole visible light spectrum. All tested FPs were capable of generating a strong LD contrast, albeit with unexpected differences and similarities between FLIPs using different FPs. A particularly notable kind of contrast was observed in KB1753-cpmTurq2-HRas, which showed opposite signs of LD in absence and in presence of Gαi1*, allowing simple, unambiguous visual identification of different conformational states of the FLIP even without LD quantitation.

Observing activation of Gαi1

We then explored whether the FLIPs that showed distinct LD in absence and presence of Gαi1* can also report on activation and inactivation of non-modified Gαi1 (Fig. 3). To ensure close to equimolar concentrations, we overexpressed a KB1753-based FLIP, as well as non-modified G proteins Gαi1, Gβ1, Gγ2 and the μ-opioid receptor (μOR). Prior to activation of the receptor, all three tested FLIPs (KB1753-eGFP-HRas, KB1753-cpmTurq2-HRas and KB1753-mScarlet-HRas) exhibited LD somewhat higher than that of the probes overexpressed alone (Fig. 3). This is likely due partially to basal activity of μOR and other Gi-coupled GPCRs present in the cells, and partially to non-specific binding of KB1753 to the non-activated form of Gαi1. Upon addition of DAMGO, a full μOR agonist[21], the LD of all three probes quickly changed, in a direction consistent with our observations of the effects of Gαi1*. Cells expressing KB1753-cpmTurq2-HRas often changed the sign of LD (LD inversion, or LD 'flip'), allowing easy visual identification of different functional states of Gαi1. The responses of all three FLIPs were smaller than what could be expected from our experiments with Gαi1*, likely due to incomplete activation of the Gαi1 pool by μOR. Upon addition of an excess of a μOR antagonist (naloxone)[16], the LD of all three FLIPs returned to values close to those observed prior to μOR activation, with residual responses attributable to

continuous presence of DAMGO. The observed responses to μOR activation/inactivation suggest that the binding of the FLIP to the activated Gαi1 does not substantially affect the kinetics of the G protein activation or inactivation. Our results show that FLIPs can be used for real-time single-cell imaging, with subcellular resolution, of activation and inactivation of non-modified, overexpressed G proteins.

To investigate whether FLIPs can report on activity of endogenously expressed Gαi proteins, we observed cells overexpressing a FLIP and μOR (allowing reliable Gαi activation), but expressing G proteins endogenously (Fig. 3d). Our results show that the LD of KB1753-eGFP-HRas and KB1753-cpmTurq2-HRas changes significantly both upon μOR activation by DAMGO and inactivation by naloxone. Unlike the other two FLIPs, KB1753-mScarlet-HRas showed no statistically significant changes in LD upon activation/ inactivation of endogenously expressed Gαi, even after observing over 50 cells.

The LD changes observed in cells overexpressing μOR and KB1753-eGFP-HRas or KB1753-cpmTurq2-HRas are in line with those we observed in cells that also overexpressed Gαi1, Gβ1 and Gγ2, but markedly smaller. Based on our measurements of LD in cells expressing Gαi1*, we estimate that about 15 % of the FLIP molecules become bound to the endogenous Gαi upon activation. In theory, reducing the molar excess of the FLIP over the endogenous Gi might lead to a larger fraction of the FLIP becoming bound upon Gi activation, and in turn, to a larger and more easily discernible change in LD. However, since we did not notice any relationship between the magnitude of the LD change and the FLIP expression level, we believe that the potential benefit of a lower FLIP concentration is being negated by the relatively low affinity of KB1753 for the activated Gαi subunits (Kd = ~1 μM)[17]. Improving the sensitivity of detection of endogenous G protein signaling will likely require increasing the affinity of the FLIP binding moiety. Despite the limits imposed by the affinity of KB1753, our ability to image activation of non-modified, endogenously expressed G proteins exceeds the best existing approaches, and is likely to improve further with future developments.

Observing activation of GPCRs

Encouraged by our observations of Gαi1 activity, we explored using FLIPs to observe activity of GPCRs. The versatility of FLIP design allowed us to create biosensors based on nanobodies NB33 and NB80, which specifically bind the activated forms of μOR and the β2-adrenergic receptor (β2AR), respectively[3,22] (Fig. 4). Briefly, the LD of NB33-eGFP-HRas exhibited rapid LD inversion upon addition of DAMGO. The response could be reversed by application of naloxone. NB80-eGFP-HRas responded to activation of β2AR (by isoproterenol) by rapid LD inversion. In fact, the observed LD change was so fast (< 100 ms) and pronounced that it could often be observed during the acquisition of a single frame by the laser scanning microscope (Fig. 4c). In contrast, the observed rate of β2AR inactivation by a β2AR inverse agonist (propranolol) was on the order of minutes. We reasoned that the high binding affinity of NB80 for β2AR (reported to be 3 nM for the isoproterenol-activated receptor[3]) was preventing the receptor from leaving the active conformation. Thus, guided by the known structure of the β2AR-NB80 complex[23] (PDB ID 3P0G), we mutated four amino acids of NB80 that form contacts with the active form of β2AR, but away from the loop that fits into the central cavity of the activated receptor (Fig 4d). The resulting FLIP, which we term NB80Lite-eGFP-HRas, exhibits optical

176 properties similar to NB80-eGFP-HRas, but virtually no affinity for the non-activated β2AR, and a
177 much faster response to β2AR inactivation (a few seconds). The large magnitude of the probe's
178 responses preserves the ability to unambiguously recognize the state of the β2AR by imaging
179 over a period of tens milliseconds (as shown in Fig 4c for NB80-eGFP-HRas) or, if scanning a small
180 area, over tens of microseconds.
181 Our results demonstrate that FLIPs can be used for sensitive, real-time observations of
182 activity of non-modified GPCRs. They also show that nanobodies can serve as affinity moieties in
183 FLIPs, while highlighting the importance of a suitable binding affinity of the FLIP for its target.
184 Lowering the binding affinity by mutating key residues yielded a probe capable of fast and
185 sensitive detection of both β2AR activation and inactivation. In combination with our
186 observations of KB1753-based probes, our results with NB80-based FLIPs place limits on the
187 range of binding affinities suitable for FLIP applications (likely 10-100 nM, depending on the
188 target concentration).
189
190
191 **Observing activity of other proteins**
192 To explore the versatility of the FLIP design and a range of applications, we developed
193 FLIPs containing the RH domain of GRK2 (known to bind the activated form of Gαq[24]), nanobody
194 NB35 (known to bind the activated form of Gαs[23]); the C-terminal domain of GRK2 (known to
195 bind the Gβγ dimer often released upon activation of G protein heterotrimers[24]), PAK1 (known
196 to bind the activated form of the small GTPase RacA[25]), as well as a recently developed GP2-
197 derived small affinity protein known[26] to bind to the ectodomain of the insulin receptor 1 (IR1)
198 (Fig. 5). Presence of their respective targets generally increased LD (that is, it increased the
199 absolute values of the observed dichroic logratios), consistent with lowering the orientational
200 freedom of the fluorescent moiety. Interestingly, GP2(1)-meGFP-CD59, a probe of activation of
201 the insulin receptor, showed intracellular localization in absence of its target, despite containing
202 a leader sequence and a GPI anchor (derived from the protein CD59[27]). In contrast, the probe
203 localized to the cell membrane in cells overexpressing both the probe and IR1. Upon addition of
204 insulin, the LD of the probe decreased, consistent with insulin-induced conformational changes
205 in the IR1 ectodomain.
206 These observations illustrate the potential range of FLIP applications, which include
207 studies of various G protein activities (Gαq, Gαs, Gβγ), function of small GTPases (activation of
208 RacA, critical for embryonic development), or activity of receptor tyrosine kinases (i.e., IR1, of
209 crucial importance in diabetes). The results also show how wide a range of molecules can serve
210 as binding moieties in FLIPs: peptides, nanobodies and nanobody-like affinity scaffolds, but also
211 natural binding partners (GRK2, PAK1) of the target proteins. Conveniently, by virtue of being
212 natural binding partners of endogenously expressed targets, such molecules are likely to exhibit
213 affinities suitable for observations of targets expressed endogenously. Thus, our results open an
214 avenue to observations of an exceedingly wide range of non-modified, endogenously expressed
215 signaling molecules.
216
217
218 **Endocytosis-associated rearrangement of GPCR–arrestin complexes**

219 Among valuable potential FLIP targets are also arrestins. Arrestins play an important role
220 in GPCR signal transduction, complementing or competing with signaling by G proteins[28]. The
221 relative involvement of G proteins and arrestins upon GPCR activation is shaped by the agonist
222 (so-called biased agonism)[29]. The roles of G proteins and arrestins are compartmentalized, both
223 spatially (cell membrane vs. endosomes) and temporally (so-called first vs. second wave of GPCR
224 signaling)[30]. Upon GPCR activation, arrestins can bind to the receptor's phosphorylated C-
225 terminus (partial engagement), or to both the C-terminus and the GPCR's central cavity (full
226 engagement)[31,32]. Partial arrestin engagement might allow formation of GPCR–G protein–
227 arrestin supercomplexes, whose existence has, however, only been demonstrated with purified,
228 reconstituted proteins, under highly favorable conditions[33]. In contrast, our approach promised
229 real-time observations of arrestin molecular interactions in living cells, with subcellular
230 resolution.
231 In order to detect interactions of arrestins with GPCRs, we prepared NB32-eGFP-HRas.
232 This FLIP utilizes NB32, a nanobody specific for activated arrestins bound to the phosphorylated
233 C-terminus of a GPCR[31]. To stimulate arrestin recruitment, we used the bradykinin receptor 2
234 (B2R) [4,34,35]. Cells overexpressing non-modified B2R, β-arrestin 1 (βArr1) and NB32-eGFP-HRas
235 responded to activation by bradykinin by an increase in LD of the probe in the cell membrane
236 (Fig. 5b, c). This likely corresponds to the formation of the fully engaged B2R–βArr1 complex.
237 Membrane vesicles (endosomes), which formed upon internalization of the activated B2R,
238 exhibited LD similar to that observed in the cell membrane of the activated cells. Thus, NB32-
239 eGFP-HRas can detect activation of βArr1 both in the cell membrane and in endosomes.
240 To test whether NB32-meGFP-hRas can distinguish between different modes of arrestin
241 binding to activated GPCRs, we prepared a βArr1 mutant (βArr1(FLD)), bearing a deletion of the
242 finger-loop region. Such deletions have been shown[31] to reduce (but not completely abolish) the
243 formation of the fully engaged GPCR–arrestin complex, enhancing arrestin's partial engagement
244 with the GPCR. In presence of βArr1(FLD), activation of B2R leads to an increase in LD of NB32-
245 eGFP-HRas present in the cell membrane similar to that observed in presence of non-mutated
246 βArr1. However, strikingly, upon internalization into endosomes, the LD of the probe undergoes
247 an inversion. This is in contrast to the behavior observed with non-mutated βArr1, and likely
248 corresponds to formation of partially-engaged complexes of B2R with βArr1(FLD).
249 The endocytosis-associated LD inversion observed with βArr1(FLD) is robust and highly
250 reproducible, and seems to occur irrespective of the endosome size (for vesicles of diameters 0.5
251 – 2 µm; Suppl. Fig. 4), cellular localization (periplasmic/intracellular; Fig. 5c), expression levels
252 (weakly/brightly fluorescent; Fig. 5c) or vesicle age (nascent/mature). Possible causes for the
253 observed conformational change include B2R's interactions with the caveolin-[36,37] or clathrin-
254 associated[38,39] endocytosis machinery, effects of the endosomal lipid composition[40], pH,
255 membrane curvature[41], or a yet-to-be-identified process occurring during the formation of
256 endosomes. Although all of these mechanisms are expected to act both on B2R–βArr1 and B2R–
257 βArr1(FLD), we could only observe rearrangement in the latter. This might reflect a true
258 difference in behaviors between βArr1 and βArr1(FLD). However, we cannot exclude that NB32
259 artificially stabilizes the fully engaged form of the B2R–βArr1 complex. In any case, our
260 observations suggest that a rearrangement occurs in complexes between GPCRs and βArr1 of
261 suitable affinities[4]. Thus, some GPCRs may be prone to undergoing this transition, while others
262 may not. Therefore, the observed conformational transition represents a potential bifurcation of

263 GPCR signaling pathways. Importantly, for reasons that are to be elucidated, this transition occurs
264 only in endosomes, not in the cell membrane. Intriguingly, the conformational transition is
265 consistent with proposed mechanisms[33] of second-wave GPCR signaling that involve
266 supercomplexes GPCR–G protein–arrestin.
267 Our observations of a previously unseen endocytosis-associated rearrangement of a
268 GPCR–arrestin complex demonstrate the capacity of FLIPs and LD microscopy to visualize
269 interactions between non-modified GPCRs and arrestins with subcellular resolution. Importantly,
270 they also illustrate a unique ability to distinguish between distinct forms of protein-protein
271 interactions. This ability, combined with the fact that the FLIP targets bear no modifications,
272 opens doors to revealing hidden aspects of cell signaling, under conditions markedly closer to
273 natural than previously possible.
274
275
276 ## Conclusions
277
278 Our results demonstrate the potential of using optical directionality of fluorescent
279 molecules for design of genetically encoded fluorescent biosensors. Despite being known for
280 decades[5], optical directionality of fluorescent proteins has remained largely overlooked as a
281 useful detection principle, due to lack of suitable molecular designs. By identifying FLIPs, a large,
282 widely applicable and exceedingly simple class of molecules capable of reporting on numerous
283 scientifically and pharmacologically important molecular processes of cell signaling, we hope to
284 open a new avenue to developing better genetically encoded biosensors.
285 The FLIP design offers a powerful combination of desirable properties. The readout is
286 quantifiable and inherently ratiometric. The probes use a single excitation/emission spectral
287 channel, allowing multiplexing. The molecular targets do not need to be modified in any way, and
288 the approach is sensitive enough to detect even activity of endogenously expressed proteins. A
289 single FLIP can report on the presence or absence of a target (such as a GPCR–arrestin complex),
290 but, uniquely, it can also distinguish among several states of the target, yielding more information
291 than other types of biosensors, even though none of the signaling molecules bear any
292 modification.
293 The FLIP design does present some limitations. LD observations rely on the shape of the
294 cell membrane, which can be irregular. However, due to the mathematical relationship between
295 LD and cell membrane orientation, accurate $\log_2(r_{max})$ determinations can be made[42] even using
296 a very small suitable section of a cell membrane. Another apparent FLIP limitation is the
297 requirement for the target to be membrane-associated. However, suitably designed FLIPs should
298 respond even to presence or absence of a cytoplasmic target, rendering this reservation largely
299 mute. It could be argued that FLIPs are partly interchangeable with translocation-based
300 biosensors. However, protein translocation is slower, difficult to accurately quantify, does not
301 yield structural information about the biosensor, and, therefore, a single translocation biosensor
302 cannot distinguish among multiple states of the target. In fact, translocation biosensor uses are
303 more strictly limited to membrane-associated targets than those of FLIPs. Finally, by binding to
304 their targets, FLIPs might sequester the targets from downstream signaling. Nonetheless,
305 choosing a suitable combination of FLIP concentration and binding affinity should allow

overcoming this drawback. Therefore, FLIPs, in combination with polarization microscopy, present a substantial, widely applicable improvement over existing approaches.

In order to observe FLIPs, various polarization microscopy implementations can be used. Our preferred FLIP imaging modality is linear dichroism microscopy, implemented on a laser-scanning confocal microscope[42]. This implementation combines the advantages of optical sectioning, a wide range of detection channels, and relatively (in comparison with fluorescence polarization microscopy) low depolarization by the objective lens and by the excited FP molecules[43]. Nonetheless, our results show that FLIPs can also be used with fluorescence polarization microscopy. Combining FLIPs with various other polarization microscopy modalities (including wide-field[44], multipoint[45], holographic[46], or super-resolution[47]), as well as with a growing range of publicly available software tools for polarization microscopy image analysis[42,48-51], promises to allow functional imaging in an excitingly wide range of biological contexts, from single-molecule studies in individual organelles or cellular compartments to large scale observations in intact tissues or animals.

In summary, we have demonstrated a wide range of applications of FLIPs to high profile molecular targets including GPCRs, G proteins, small GTPases, receptor tyrosine kinases and arrestins. The targets do not bear any modifications, and can even be endogenously expressed, representing a major advantage in our imaging abilities over existing approaches[2,8,16]. Using one of our FLIPs, we identified a pronounced conformational change in GPCR-arrestin complexes, and showed that it occurs specifically in endosomes, bringing a new insight into mechanisms of signaling by GPCRs, an exceedingly large and important class of proteins. The ability to observe this conformational change in living cells, in real time, in signaling proteins that have not been modified in any way, sets a new standard in microscopy imaging of protein signaling.

By allowing innumerable combinations of affinity binders, anchoring moieties, linkers and fluorescent molecules (potentially including self-labeling proteins), the FLIP design allows rapid development of a wide variety of new molecular biosensors. Furthermore, by drawing attention to optical directionality of fluorescent proteins, our results will likely inspire other biosensor designs that take advantage of this fundamental property of fluorescent molecules. We hope that the present work will ultimately transform polarization-resolved fluorescence microscopy, a simple, long overlooked optical microscopy modality, into a mainstream tool of functional biomolecular imaging.

339
340
341
342

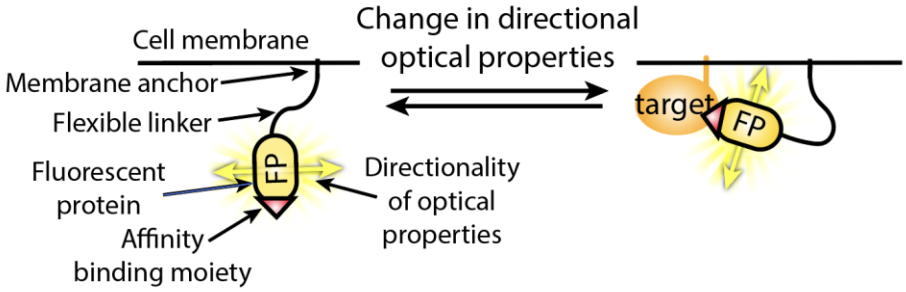

343
344 **Figure 1: General design of fluorescence anisotropy and linear dichroism probes (FLIPs).**
345
346
347

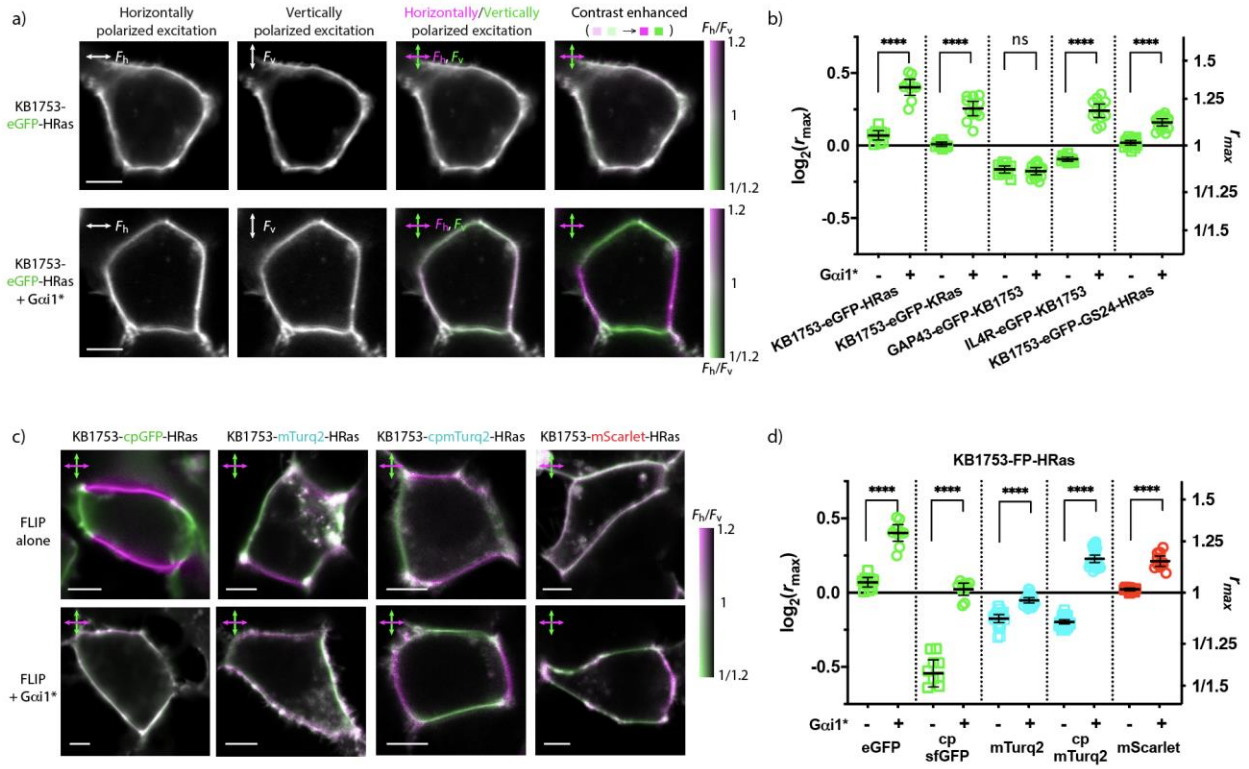

Figure 2: Detecting the presence of a constitutively active mutant of Gαi1 (Gαi1*) by FLIPs and LD microscopy. a) A HEK293 cell expressing KB1753-eGFP-HRas (top) and coexpressing KB1753-eGFP-HRas and Gαi1* (bottom). From left to right: image acquired using excitation light polarized horizontally; image acquired using excitation light polarized vertically; the two preceding images colored magenta and green, respectively, and overlaid; same as in the preceding image, but the coloring adjusted to cover the shown range of dichroic ratios (F_h/F_v,), as indicated by the color bar. In cells expressing Gαi1*, the FLIP exhibits pronounced LD. Scale bars: 5 µm. **b)** LD of eGFP-bearing FLIPs containing various membrane anchors and linkers, in absence and presence of Gαi1*. Means and 95% confidence intervals are indicated. With the exception of GAP43-eGFP-KB1753, all tested FLIPs exhibit significantly different LD in presence of Gαi1*. **c)** Representative LD microscopy images of HEK293 cells expressing FLIPs of the KB1753-FP-HRas design, bearing various FPs. Coloring as in **a**. Scale bars: 5 µm. Top: cells expressing the indicated FLIP; bottom: cells co-expressing the indicated FLIP and Gαi1*. Differences in LD between cells expressing only a FLIP and co-expressing the FLIP and Gαi1* are apparent. Notably, cells expressing KB1753-cpmTurq2-HRas exhibit LD of a different sign in absence and presence of Gαi1* (inversion of the magenta-green pattern). **d)** LD of FLIPs of the KB1753-FP-HRas design, bearing different FP moieties. Means and 95% confidence intervals are indicated. Presence of Gαi1* had a significant effect on the LD of all tested FLIPs. Marked differences between the distinct FLIPs are apparent.

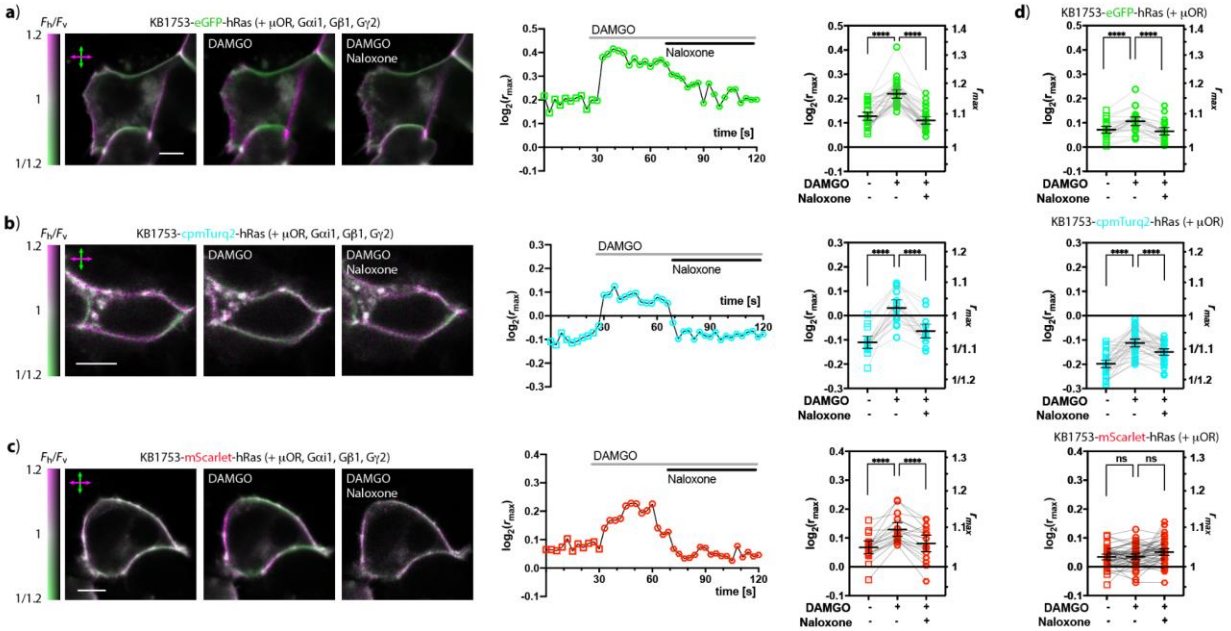

Figure 3: Imaging activity of Gαi1 by LD microscopy and FLIPs of the KB1753-FP-HRas design. a-c) HEK293 cells overexpressing the μ-opioid receptor (μOR), Gαi1, Gβ1, Gγ2 and the indicated FLIP, imaged before and after addition of a μOR agonist (DAMGO), and after addition of an excess μOR antagonist (naloxone). **a)** KB1753-eGFP-HRas; **b)** KB1753-cpmTurq2-HRas; **c)** KB1753-mScarlet-HRas. Left: LD microscopy images showing a cell before addition of DAMGO, after addition of DAMGO, and after addition of naloxone. All scale bars 5 μm. Middle: temporal profile of LD in response to μOR activation and inactivation of the shown cell. Right: LD of cells prior to activation, 30 s after addition of DAMGO, and 30 s after addition of naloxone. Changes in LD in response to addition of DAMGO and naloxone are apparent for all three FLIPs. **d)** LD of HEK293 cells overexpressing μOR and the indicated KB1753-FP-HRas (not overexpressing any G protein), before and after addition of DAMGO and after addition of naloxone. Mean values and 95% confidence intervals indicated.

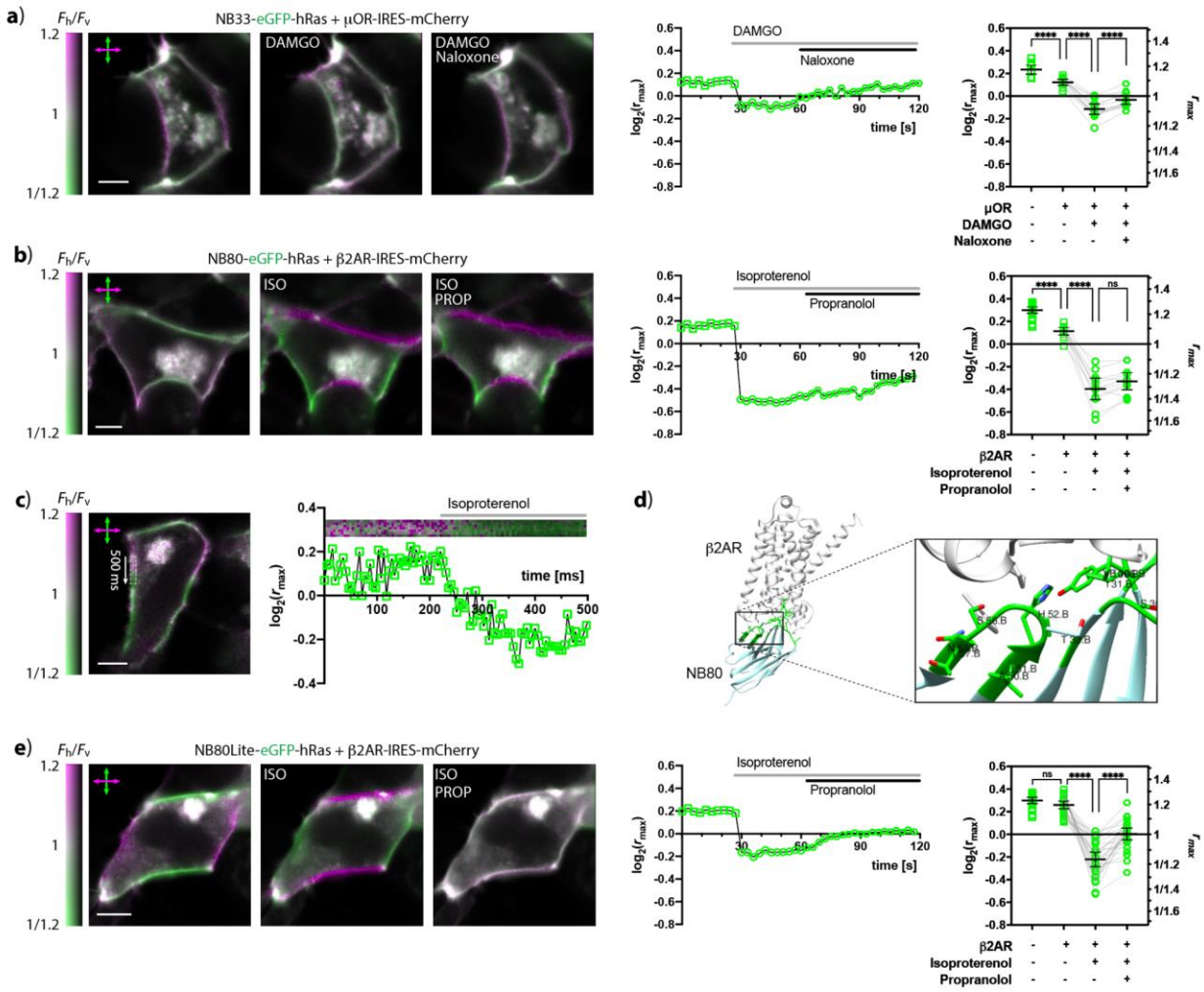

Figure 4: Imaging GPCR activity by LD microscopy and FLIPs. a) Imaging μOR activity in HEK293 cells overexpressing μOR-IRES-mCherry and NB32-eGFP-HRas. Left: A cell observed before stimulation, after μOR activation (by addition of DAMGO), and after μOR inactivation (by addition of naloxone); Middle: temporal profile of LD during μOR activation and inactivation of the shown cell; Right: values of LD observed in absence of μOR, and in its presence before stimulation, 30 s after activation, and 30 s after inactivation (each data point represents a single cell; mean values and 95 % confidence intervals indicated). **b)** β2AR activity in HEK293 cells overexpressing β2AR-IRES-mCherry and NB80-eGFP-HRas; isoproterenol (ISO) and propranolol (PROP) were used for β2AR activation and inactivation, respectively. **c)** An NB80-eGFP-HRas response during acquisition of a single image. Left: an image of a cell imaged during agonist delivery, showing an LD inversion occurring while the image was being acquired; Right: a temporal profile of the LD inversion in the indicated region of the image on the left. **d)** Structure of the β2AR-NB80 complex (PDB ID 3P0G) showing the loop region of NB80 mutated to create NB80Lite. Residues of NB80 forming contacts with β2AR are shown in green. **e)** Imaging β2AR activity using NB80Lite-eGFP-HRas. All scale bars 5 μm.

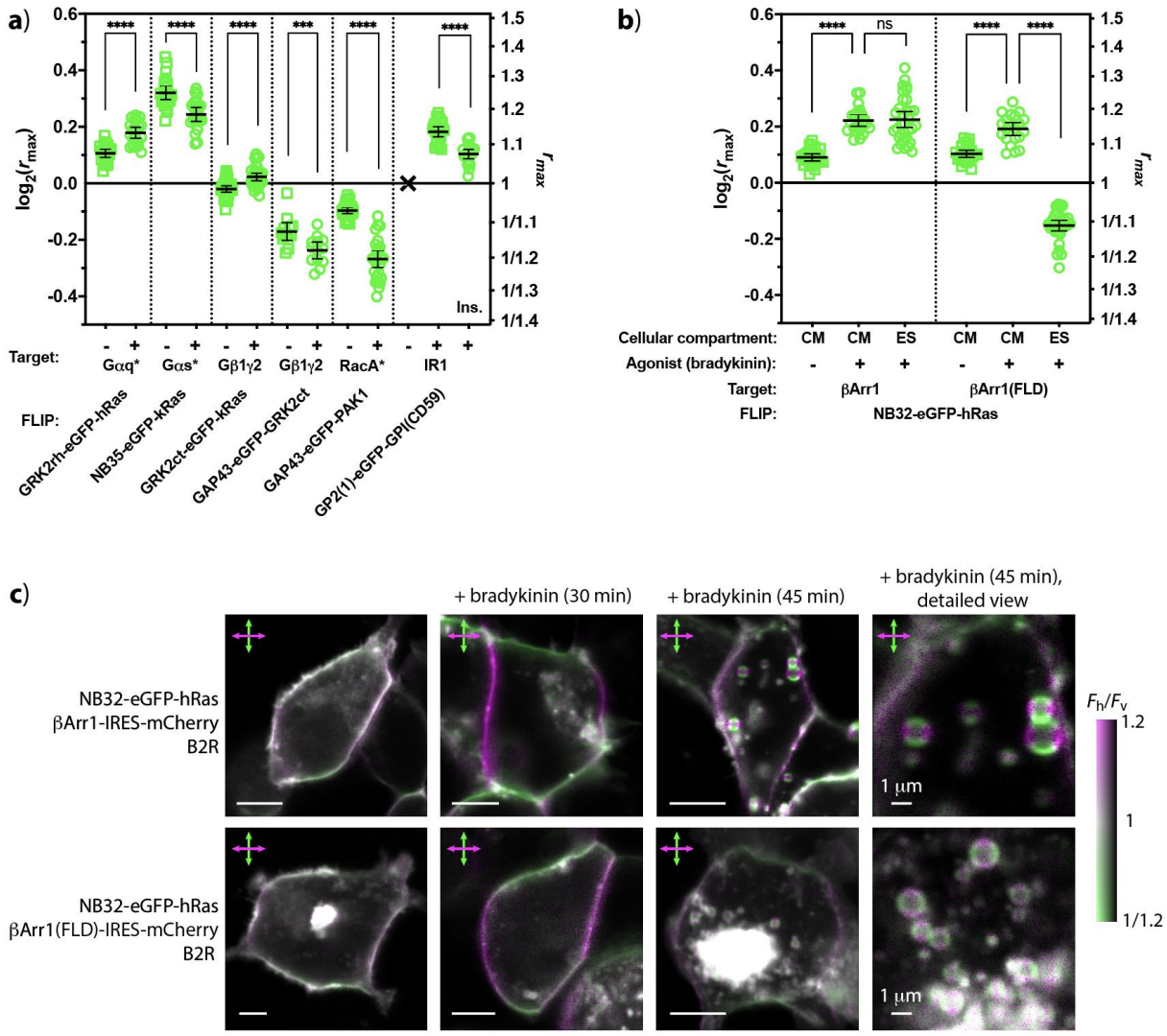

Figure 5: Other FLIPs. a) Results of LD microscopy observations of various FLIPs, in absence and in presence of their targets, namely the Gα subunits Gαq and Gαs, the Gβ1γ2 dimer, the small GTPase RacA, and the insulin receptor 1 (IR1). Constitutively active mutants indicated by an asterisk (*). Stimulation by insulin (Ins.) indicated. Each data point represents a single cell; a cross (x) indicates poor membrane localization; mean values and 95 % confidence intervals are shown. **b)** Observations of NB32-eGFP-hRas in response to arrestin activation/recruitment due to stimulation of the bradykinin receptor (B2R) by bradykinin. Cells overexpressing β-Arrestin1 (βArr1) and its finger-loop deletion mutant βArr1(FLD) exhibit similar LD responses in the cell membrane (CM), but markedly different responses in endosomes (ES) that emerge upon prolonged activation. **c)** Images of typical cells overexpressing B2R, NB32-eGFP-hRas, and βArr1 (top row) or βArr1(FLD) (bottom row). From left to right: before application of bradykinin; 30 min after application of bradykinin; 45 min after application of bradykinin; and a detailed view showing endosomes, 45 min after application of bradykinin. Scale bars: 5 µm unless indicated otherwise.

423 **Methods**
424 Constructs:
425 The plasmids encoding KB1753-eGFP-HRas and GAP43-eGFP-KB1753 (both in the pcDNA3.1(+)
426 backbone) were prepared by gene synthesis (GenScript). The constructs were designed to allow
427 excision of the DNA encoding the affinity binding moiety, the FP moiety, and the membrane-
428 targeting moiety by a unique combination of restriction endonucleases (EcoRI/XhoI, XhoI/BamHI
429 and BamHI/NotI, respectively). Other FLIPs were prepared from the two starting plasmids by a
430 suitable restriction digestion, followed by ligation of the desired DNA fragment, obtained through
431 gene synthesis (GenScript). As fluorescent proteins we used eGFP bearing the dimerization-
432 preventing mutations A206K, L221K and F223R. Circularly permuted FPs (cpmTurq2, cpsfGFP)
433 were based on superfolder mTurquoise2 and sfGFP2. FLIP targets were cloned into a pcDNA3.1(+)
434 plasmid backbone containing either IRES-mCherry or IRES-mTurquoise2, allowing identification
435 of target-expressing cells by fluorescence of the bicistronically expressed FP, while the targets
436 themselves bore no modifications. Constitutively active mutants (Gαi1(Q204L)), Gαq(Q209L),
437 Gαs(Q227L), RacA(Q61L)) were prepared by PCR mutagenesis. NB80Lite was created by
438 introducing mutations H52S, S56G, T57S and N58A into NB80-eGFP-HRas by PCR mutagenesis.
439
440 Mammalian cell culture:
441 HEK293 cells obtained from ATCC, passaged less than 15 times were used throughout. Cells were
442 regularly tested for mycoplasma by Hoechst staining. For imaging, cells were plated in 8- or 18-
443 well imaging slides (iBidi) and transfected with the desired plasmid (0.5 µg per well) using
444 Lipofectamine 3000 (Thermo Fisher) and the manufacturer's procedure. Cells were observed by
445 LD microscopy 1 or 2 days after transfection. During imaging, GPCR agonists (DAMGO,
446 isoproterenol, bradykinin; final concentrations 10 µM) and antagonists (naloxone, proterenol;
447 final concentrations 100 µM) were added by manual pipetting. Agonists and antagonists were
448 purchased from Sigma-Aldrich.
449
450 Microscopy
451 LD imaging was carried out as described previously[8,42], on a customized laser scanning confocal
452 microscope (Olympus FV1200), equipped with a polarization modulator (RPM-2P, Innovative
453 Bioimaging, L.L.C.) alternating the excitation light linear polarization between acquisition of
454 subsequent pixels by the microscope. The objective (UApoN340, NA1.15, Olympus, Japan) and
455 pixel dwell times of 10 µs were used throughout. Cells expressing constructs bearing mTurqoise2
456 were imaged using 405 nm illumination and a 450-550 nm emission window. Cells expressing
457 constructs containing eGFP were imaged using 488 nm illumination, and emission 510-610 nm
458 was collected. Cells expressing constructs with mScarlet and mCherry were imaged using 543 nm
459 excitation; emission 560-650 nm was collected. The resulting images were processed and
460 analyzed as described[42], using Fiji and publicly available macros for LD image analysis, as well as
461 Polaris+ software (Innovative Bioimaging, L.L.C.). Briefly, each raw image (containing information
462 on fluorescence intensity acquired with both excitation polarizations) was deconvolved into a
463 pair of images, each holding information on fluorescence intensity acquired with one polarization
464 of the excitation light. For LD visualization, the images acquired with horizontal and vertical
465 polarization of the excitation light were colored magenta and green, respectively, and the color
466 saturation was adjusted to match the desired range of LD. To quantitate LD, parts of images

containing the cell membrane were semi-automatically segmented, and the shape of the cell outline was approximated by a spline. For each segmented pixel, the dichroic logratio ($\log_2(r) = \log_2(F_h/F_v)$) and membrane orientation (angle θ; slope at the nearest point on the spline approximating the cell outline) were determined as described previously[42]. At least ten cells were observed and analyzed for each construct or combination of constructs, over at least three different weeks. Distributions of the $\log_2(r_{max})$ values for a large majority of our experiments were normal (according to Anderson-Darling, D'Agostino & Pearson tests). To maintain consistency, we treated all $\log_2(r_{max})$ values as normally distributed.

Fluorescence polarization imaging was carried out using a modified Olympus FV1200 confocal microscope. For illumination, the optical fiber with a collimator was detached from the microscope body, and a Glan-Taylor polarizer (GT10-A, Thorlabs) and an achromatic quarter-wave plate (WP140HE, Edmund Optics) oriented to ensure circularly polarized sample illumination were placed in the laser beam path before the beam was steered into the scanning unit. In the detector unit, a dichroic beam splitter assembly was replaced by a polarizing beam splitter cube (PBS201, Thorlabs) flanked by sheet polarizers (XP42, Edmund Optics, extinction ratio 9000:1). To allow comparisons with observations of linear dichroism, the extent of fluorescence polarization was quantified analogously, by observing the logratio of the two fluorescence intensities along the cell outline and determining, by fitting, the maximum value ($\log_2(r_{max})$), corresponding to the value of $\log_2(F_{\parallel}/F_{\perp})$ at membrane sections oriented horizontally in the image (θ = 0).

Acknowledgements

The research was supported by Ministry of Education, Youth and Science of the Czech Republic grant LTAIN19167 (J.L.) and EIC PathFinder project UniSens (J.L.). Data storage was provided by the CESNET LM2015042 facility under the program "Large Research, Development, and Innovation Infrastructures." We appreciate the help of Z. Vaitova with preparing constructs and performing microscopy imaging and the help of P. Khoroshyy with microscopy equipment. We thank P. Dedecker (KU Leuven) for support and for editing the manuscript. We thank M. Garcia-Marcos (U. Boston) for providing constructs for preliminary experiments.

Author contributions

P. M. designed and prepared constructs, carried out microscopy imaging, data processing and analyses, and contributed to writing the paper. V.M. performed imaging, data processing and analyses. A.S. developed and investigated FLIPs of IR activity. A.B. inspired the idea of FLIPs and supervised experiments. J.L. provided technical expertise, directed and managed the project, and wrote the manuscript, with input from the other co-authors.

508 **Microscopy data summary:**

509

Construct(s), agonists, antagonists	Number of observed cells	Linear dichroism $Log_2(r_{max})$ (mean ± 2SEM)
KB1753-eGFP-HRas	10	0.07 ± 0.03
KB1753-eGFP-HRas + $G\alpha i_1$(Q204L)-IRES-mCherry	10	0.40 ± 0.05
KB1753-eGFP-KRas	10	0.01 ± 0.01
KB1753-eGFP-KRas + Gαi1(Q204L)-IRES-mCherry	12	0.26 ± 0.04
GAP43-eGFP-KB1753	12	-0.16 ± 0.02
GAP43-eGFP-KB1753 + Gαi1(Q204L)-IRES-mCherry	15	-0.18 ± 0.02
IL4R-eGFP-KB1753	10	-0.09 ± 0.01
IL4R-eGFP-KB1753 + Gαi1(Q204L)-IRES-mCherry	12	0.24 ± 0.02
KB1753-eGFP-GS15-HRas	15	0.05 ± 0.02
KB1753-eGFP-GS15-HRas + Gαi1(Q204L)-IRES-mCherry	16	0.30 ± 0.03
KB1753-eGFP-GS20-HRas	12	0.03 ± 0.01
KB1753-eGFP-GS20-HRas + Gαi1(Q204L)-IRES-mCherry	15	0.26 ± 0.03
KB1753-eGFP-GS24-HRas	15	0.02 ± 0.01
KB1753-eGFP-GS24-HRas + Gαi1(Q204L)-IRES-mCherry	15	0.16 ± 0.02
KB1753-cpsfGFP-HRas	10	-0.54 ± 0.08
KB1753-cpsfGFP-HRas + Gαi1(Q204L)-IRES-mCherry	10	0.02 ± 0.03
KB1753-mTurq2-HRas	20	-0.17 ± 0.03

KB1753-mTurq2-HRas + Gαi1(Q204L)-IRES-mCherry	20	-0.05 ± 0.02
KB1753-cpmTurq2-HRas	26	-0.20 ± 0.01
KB1753-cpmTurq2-HRas + Gαi1(Q204L)-IRES-mCherry	26	0.23 ± 0.02
KB1753-mScarlet-HRas	10	0.02 ± 0.01
KB1753-mScarlet-HRas + Gαi1(Q204L)-IRES-mTurq2	11	0.21 ± 0.03
KB1753-eGFP-HRas + μOR-IRES-mCherry + Gαi1-T2A-Gβ1-T2A-Gγ2-IRES-mCherry	34	0.13 ± 0.02
KB1753-eGFP-HRas + μOR-IRES-mCherry + Gαi1-T2A-Gβ1-T2A-Gγ2-IRES-mCherry + 10 μM DAMGO	34	0.22 ± 0.02
KB1753-eGFP-HRas + μOR-IRES-mCherry + Gαi1-T2A-Gβ1-T2A-Gγ2-IRES-mCherry + 10 μM DAMGO + 100 μM naloxone	34	0.11 ± 0.02
KB1753-cpmTurq2-HRas + μOR-IRES-mCherry + Gαi1-T2A-Gβ1-T2A-Gγ2-IRES-mCherry	17	-0.11 ± 0.02
KB1753-cpmTurq2-HRas + μOR-IRES-mCherry + Gαi1-T2A-Gβ1-T2A-Gγ2-IRES-mCherry + 10 μM DAMGO	17	0.03 ± 0.03
KB1753-cpmTurq2-HRas + μOR-IRES-mCherry + Gαi1-T2A-Gβ1-T2A-Gγ2-IRES-mCherry + 10 μM DAMGO + 100 μM naloxone	17	-0.06 ± 0.03
KB1753-mScarlet-HRas + μOR-IRES-	18	0.07 ± 0.02

mCherry + Gαi1-T2A-Gβ1-T2A-Gγ2-IRES-mCherry		
KB1753-mScarlet-HRas + μOR-IRES-mCherry + Gαi1-T2A-Gβ1-T2A-Gγ2-IRES-mCherry + 10 μM DAMGO	18	0.13 ± 0.02
KB1753-mScarlet-HRas + μOR-IRES-mCherry + Gαi1-T2A-Gβ1-T2A-Gγ2-IRES-mCherry + 10 μM DAMGO + 100 μM naloxone	18	0.08 ± 0.03
KB1753-eGFP-HRas (fluorescence polarization)	24	0.10 ± 0.02
KB1753-eGFP-HRas + $G\alpha_{i1}$(Q204L)-IRES-mCherry (fluorescence polarization)	15	0.44 ± 0.03
KB1753-eGFP-HRas + μOR-IRES-mCherry	26	0.07 ± 0.01
KB1753-eGFP-HRas + μOR-IRES-mCherry + 10 μM DAMGO	26	0.11 ± 0.02
KB1753-eGFP-HRas + μOR-IRES-mCherry + 10 μM DAMGO + 100 μM naloxone	26	0.07 ± 0.01
KB1753-cpmTurq2-HRas + μOR-IRES-mCherry	38	-0.20 ± 0.02
KB1753-cpmTurq2-HRas + μOR-IRES-mCherry + 10 μM DAMGO	38	-0.11 ± 0.02
KB1753-cpmTurq2-HRas + μOR-IRES-mCherry +	38	-0.15 ± 0.01

10 µM DAMGO + 100 µM naloxone		
KB1753-mScarlet-HRas + µOR-YFP	49	0.03 ± 0.01
KB1753-mScarlet-HRas + µOR-YFP + 10 µM DAMGO	49	0.04 ± 0.01
KB1753-mScarlet-HRas + µOR-YFP + 10 µM DAMGO + 100 µM naloxone	49	0.05 ± 0.01
NB33-eGFP-HRas	11	0.23 ± 0.04
NB33-eGFP-HRas + µOR-IRES-mCherry	14	0.12 ± 0.02
NB33-eGFP-HRas + µOR-IRES-mCherry + 10 µM DAMGO	14	-0.11 ± 0.04
NB33-eGFP-HRas + µOR-IRES-mCherry + 10 µM DAMGO + 100 µM naloxone	14	-0.03 ± 0.04
NB80-eGFP-HRas	20	0.30 ± 0.03
NB80-eGFP-HRas + β2AR-IRES-mCherry	12	0.11 ± 0.03
NB80-eGFP-HRas + β2AR-IRES-mCherry + 10 µM isoproterenol	12	-0.40 ± 0.09
NB80-eGFP-HRas + β2AR-IRES-mCherry + 10 µM isoproterenol + 100 µM propranolol	12	-0.33 ± 0.07

NB80Lite-eGFP-HRas	30	0.24 ± 0.03
NB80Lite-eGFP-HRas + β2AR-IRES-mCherry	27	0.26 ± 0.03
NB80Lite-eGFP-HRas + β2AR-IRES-mCherry + 10 μM isoproterenol	27	-0.22 ± 0.06
NB80Lite-eGFP-HRas + β2AR-IRES-mCherry + 10 μM isoproterenol + 100 μM propranolol	27	0.00 ± 0.05
GRK2rh-eGFP-HRas	20	0.11 ± 0.02
GRK2rh-eGFP-HRas + Gαq(Q209L)-IRES-mCherry	20	0.18 ± 0.02
NB35-eGFP-HRas	23	0.32 ± 0.02
NB35-eGFP-HRas + Gαs(Q227L)-IRES-mCherry + Gβ1-T2A-Gγ2-IRES-sfTurq2	21	0.24 ± 0.02
GRK2ct-eGFP-KRas	32	-0.02 ± 0.01
GRK2ct-eGFP-KRas + Gβ1-T2A-Gγ2-IRES-mCherry	31	0.02 ± 0.01
GAP43-eGFP-GRK2ct	13	-0.17 ± 0.03
GAP43-eGFP-GRK2ct + Gβ1-T2A-Gγ2-IRES-mCherry	13	-0.24 ± 0.03
GAP43-eGFP-PAK1	30	-0.10 ± 0.01
GAP43-eGFP-PAK1 + RacA(Q61L)-IRES-mCherry	26	-0.27 ± 0.03
GP2(1)-eGFP-GPI(CD59)	10	intracellular localization
GP2(1)-eGFP-GPI(CD59) + IR-OFP	20	0.18 ± 0.02
GP2(1)-eGFP-GPI(CD59) +	20	0.10 ± 0.03

IR-OFP + 10 nM insulin		
NB32-eGFP-HRas	15	0.06 ± 0.02
NB32-eGFP-HRas + B2R + β-Arrestin1-IRES-mCherry	22	0.09 ± 0.01
NB32-eGFP-HRas + B2R + β-Arrestin1-mCherry + 10 µM bradykinin (cell membrane)	22	0.22 ± 0.02
NB32-eGFP-HRas + B2R + β-Arrestin1-IRES-mCherry + 10 µM bradykinin (endosomes)	33	0.23 ± 0.03
NB32-eGFP-HRas + B2R + β-Arrestin1(FLD)-IRES-mCherry	23	0.10 ± 0.01
NB32-eGFP-HRas + B2R + β-Arrestin1(FLD)-IRES-mCherry + 10 µM bradykinin (cell membrane)	22	0.19 ± 0.02
NB32-eGFP-HRas + B2R + β-Arrestin1(FLD)-IRES-mCherry + 10 µM bradykinin (endosomes)	33	-0.15 ± 0.02

510
511

Suppl. Fig. 1: Fluorescence polarization imaging of HEK293 cells expressing KB1753-meGFP-HRas. **a)** A cell expressing KB1753-eGFP-HRas (top) and coexpressing KB1753-eGFP-HRas and Gαi1(Q204L)-IRES-mCherry (Gαi1*, bottom). From left to right: fluorescence polarized horizontally; fluorescence polarized vertically; the two preceding images colored magenta and green, respectively, and overlaid; same as in the preceding image, but the coloring adjusted to cover the shown range of fluorescence intensity ratios (F_h/F_v,), as indicated by the color bar. In cells expressing Gαi1*, the FLIP exhibits pronounced fluorescence polarization. Scale bars: 5 µm. **b)** Extent of fluorescence polarization in cells expressing KB1753-eGFP-HRas, in absence and presence of Gαi1*. Means and 95% confidence intervals are indicated. The probe exhibits significantly higher fluorescence polarization in presence of Gαi1*.

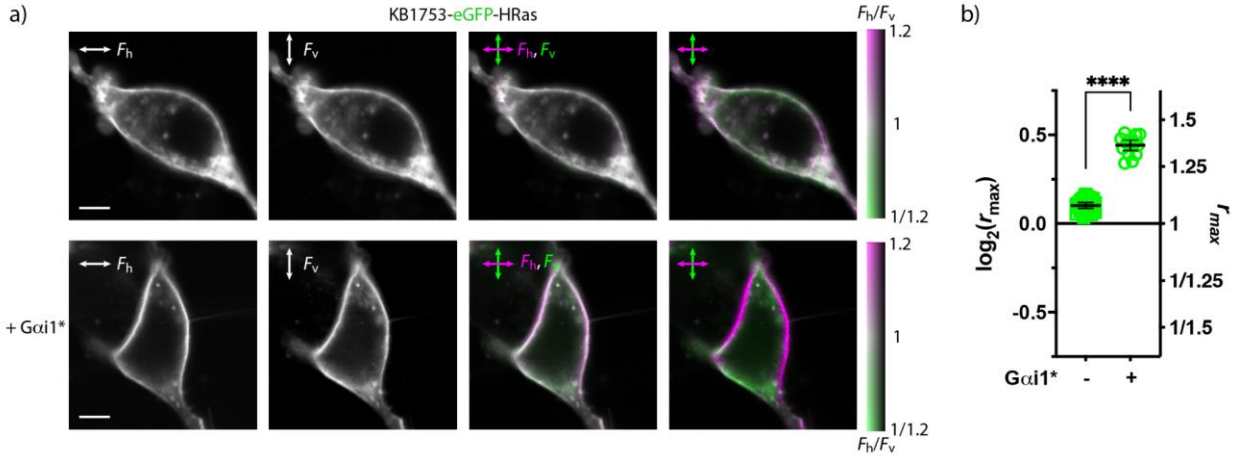

Suppl. Fig. 2: Effects of cell membrane anchors on LD of FLIPs containing the affinity binding peptide KB1753, in absence and in presence of a constitutively active mutant of Gαi1 (Gαi1*).

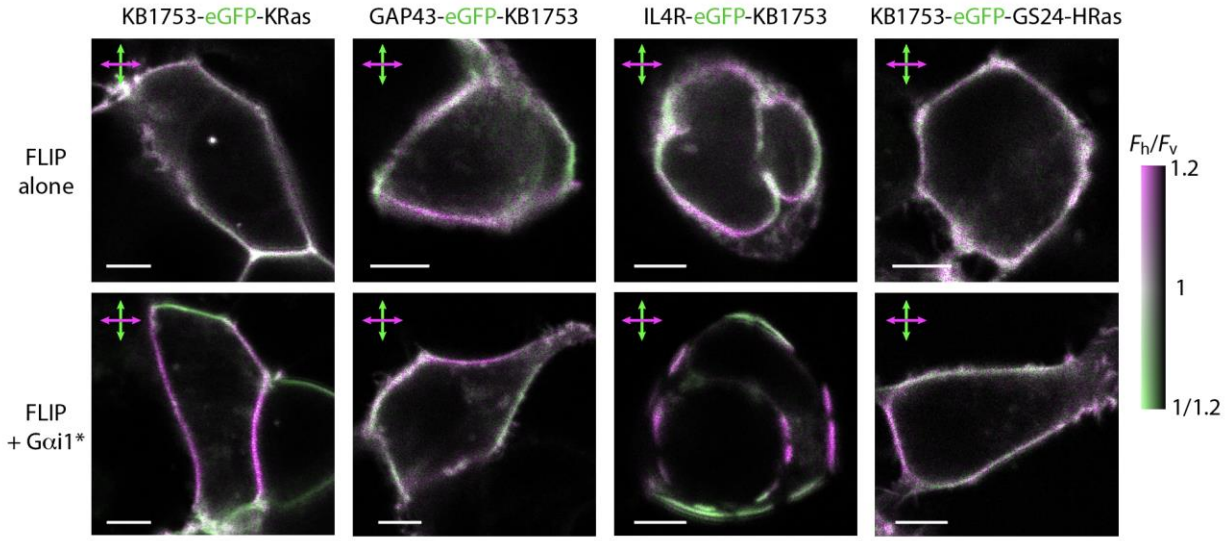

532 **Suppl. Fig. 3:** Effect of linker length in KB1753-meGFP-linker-HRas probes on their LD, in
533 absence and in presence of a constitutively active mutant of Gαi1 (Gαi1*).
534

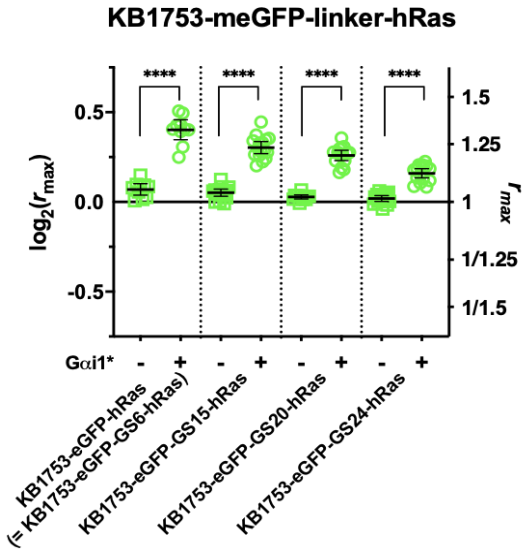

535
536
537
538
539
540
541
542 **Suppl. Fig. 4:** LD as a function of vesicle diameter in cells overexpressing B2R and βArr1-IRES-
543 mCherry, or B2R and βArr1(FLD)-IRES-mCherry.
544

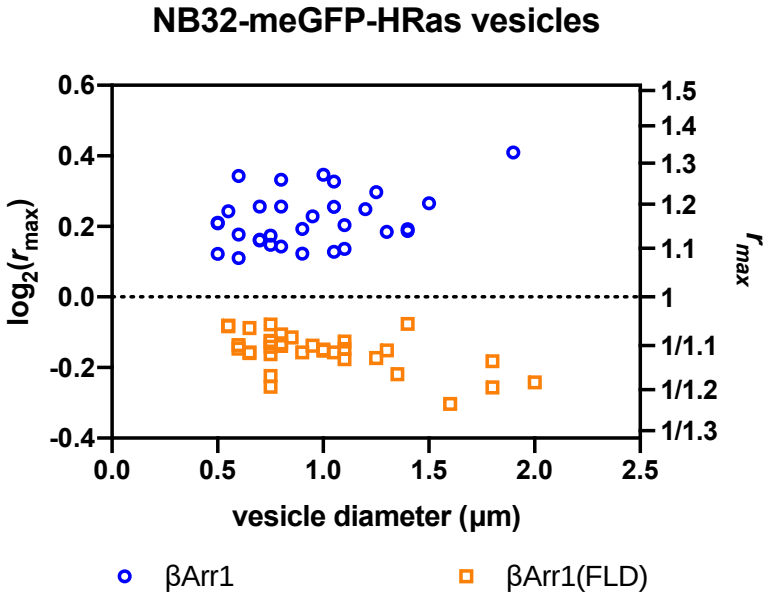

545

References:

1 Ovechkina, V. S., Zakian, S. M., Medvedev, S. P. & Valetdinova, K. R. Genetically encoded fluorescent biosensors for biomedical applications. *Biomedicines* **9**, 1528 (2021).

2 Bondar, A. & Lazar, J. Optical sensors of heterotrimeric G protein signaling. *The FEBS Journal* **288**, 2570-2584 (2021).

3 Irannejad, R. *et al.* Conformational biosensors reveal GPCR signalling from endosomes. *Nature* **495**, 534-538 (2013).

4 Avet, C. *et al.* Effector membrane translocation biosensors reveal G protein and βarrestin coupling profiles of 100 therapeutically relevant GPCRs. *Elife* **11**, e74101 (2022).

5 Inoué, S., Shimomura, O., Goda, M., Shribak, M. & Tran, P. Fluorescence polarization of green fluorescence protein. *Proceedings of the National Academy of Sciences* **99**, 4272-4277 (2002).

6 Myšková, J. *et al.* Directionality of light absorption and emission in representative fluorescent proteins. *Proceedings of the National Academy of Sciences* **117**, 32395-32401 (2020).

7 Vrabioiu, A. M. & Mitchison, T. J. Structural insights into yeast septin organization from polarized fluorescence microscopy. *Nature* **443**, 466-469 (2006). https://doi.org/10.1038/nature05109

8 Lazar, J., Bondar, A., Timr, S. & Firestein, S. J. Two-photon polarization microscopy reveals protein structure and function. *Nature Methods* **8**, 684-690 (2011). https://doi.org/10.1038/nmeth.1643

9 Han, Z. *et al.* Mechanistic studies of the genetically encoded fluorescent protein voltage probe ArcLight. *PLoS One* **9**, e113873 (2014). https://doi.org/10.1371/journal.pone.0113873

10 Valades Cruz, C. A. *et al.* Quantitative nanoscale imaging of orientational order in biological filaments by polarized superresolution microscopy. *Proc Natl Acad Sci U S A* **113**, E820-828 (2016). https://doi.org/10.1073/pnas.1516811113

11 Nakai, N. *et al.* Development of nanobody-based POLArIS orientation probes enabled multi-color/multi-target orientation imaging in living cells. *Biochemical and Biophysical Research Communications* **565**, 50-56 (2021).

12 McQuilken, M. *et al.* Analysis of septin reorganization at cytokinesis using polarized fluorescence microscopy. *Frontiers in Cell and Developmental Biology* **5**, 42 (2017).

13 Warren, S. C., Margineanu, A., Katan, M., Dunsby, C. & French, P. M. W. Homo-FRET Based Biosensors and Their Application to Multiplexed Imaging of Signalling Events in Live Cells. *International Journal of Molecular Sciences* **16**, 14695-14716 (2015).

14 Bondar, A. & Lazar, J. Dissociated GalphaGTP and Gbetagamma protein subunits are the major activated form of heterotrimeric Gi/o proteins. *Journal of Biological Chemistry* **289**, 1271-1281 (2014). https://doi.org/10.1074/jbc.M113.493643

15 Bondar, A. & Lazar, J. The G protein Gi1 exhibits basal coupling but not preassembly with G protein-coupled receptors. *Journal of Biological Chemistry* **292**, 9690-9698 (2017). https://doi.org/10.1074/jbc.M116.768127

589 16 Maziarz, M. *et al.* Revealing the activity of trimeric G-proteins in live cells with a versatile
590 biosensor design. *Cell* **182**, 770-785. e716 (2020).
591 17 Johnston, C. A. *et al.* Minimal Determinants for Binding Activated Gα from the Structure
592 of a Gαi1− Peptide Dimer. *Biochemistry* **45**, 11390-11400 (2006).
593 18 Stickney, J. T., Booden, M. A. & Buss, J. E. in *Methods in Enzymology* Vol. 332 64-77
594 (Elsevier, 2001).
595 19 Ast, C. *et al.* Ratiometric Matryoshka biosensors from a nested cassette of green-and
596 orange-emitting fluorescent proteins. *Nature Communications* **8**, 431 (2017).
597 20 Goedhart, J. *et al.* Structure-guided evolution of cyan fluorescent proteins towards a
598 quantum yield of 93%. *Nature communications* **3**, 751 (2012).
599 21 Melkes, B., Hejnova, L. & Novotny, J. Biased μ-opioid receptor agonists diversely
600 regulate lateral mobility and functional coupling of the receptor to its cognate G
601 proteins. *Naunyn-Schmiedeberg's archives of pharmacology* **389**, 1289-1300 (2016).
602 22 Stoeber, M. *et al.* A genetically encoded biosensor reveals location bias of opioid drug
603 action. *Neuron* **98**, 963-976. e965 (2018).
604 23 Rasmussen, S. G. *et al.* Structure of a nanobody-stabilized active state of the β2
605 adrenoceptor. *Nature* **469**, 175-180 (2011).
606 24 Hollins, B., Kuravi, S., Digby, G. J. & Lambert, N. A. The c-terminus of GRK3 indicates
607 rapid dissociation of G protein heterotrimers. *Cellular signalling* **21**, 1015-1021 (2009).
608 25 Park, K. C. *et al.* Rac regulation of chemotaxis and morphogenesis in Dictyostelium. *The*
609 *EMBO journal* **23**, 4177-4189 (2004).
610 26 Chan, J. Y., Hackel, B. J. & Yee, D. Targeting insulin receptor in breast cancer using small
611 engineered protein scaffolds. *Molecular cancer therapeutics* **16**, 1324-1334 (2017).
612 27 Voisin, T. B., Couves, E. C., Tate, E. W. & Bubeck, D. Dynamics and Molecular Interactions
613 of GPI-Anchored CD59. *Toxins* **15**, 430 (2023).
614 28 Van Gastel, J. *et al.* β-Arrestin based receptor signaling paradigms: Potential therapeutic
615 targets for complex age-related disorders. *Frontiers in pharmacology* **9**, 1369 (2018).
616 29 Wootten, D., Christopoulos, A., Marti-Solano, M., Babu, M. M. & Sexton, P. M.
617 Mechanisms of signalling and biased agonism in G protein-coupled receptors. *Nature*
618 *reviews Molecular cell biology* **19**, 638-653 (2018).
619 30 Tsvetanova, N. G., Irannejad, R. & von Zastrow, M. G protein-coupled receptor (GPCR)
620 signaling via heterotrimeric G proteins from endosomes. *Journal of Biological Chemistry*
621 **290**, 6689-6696 (2015).
622 31 Cahill III, T. J. *et al.* Distinct conformations of GPCR–β-arrestin complexes mediate
623 desensitization, signaling, and endocytosis. *Proceedings of the National Academy of*
624 *Sciences* **114**, 2562-2567 (2017).
625 32 Latorraca, N. R. *et al.* Molecular mechanism of GPCR-mediated arrestin activation.
626 *Nature* **557**, 452-456 (2018).
627 33 Nguyen, A. H. *et al.* Structure of an endosomal signaling GPCR–G protein–β-arrestin
628 megacomplex. *Nature structural & molecular biology* **26**, 1123-1131 (2019).
629 34 Zimmerman, B. *et al.* Role of ssarrestins in bradykinin B2 receptor-mediated signalling.
630 *Cellular signalling* **23**, 648-659 (2011).

35 Simaan, M., Bédard-Goulet, S., Fessart, D., Gratton, J.-P. & Laporte, S. A. Dissociation of β-arrestin from internalized bradykinin B2 receptor is necessary for receptor recycling and resensitization. *Cellular signalling* **17**, 1074-1083 (2005).

36 Lamb, M. E., De Weerd, W. F. & LEEB-LUNDBERG, L. F. Agonist-promoted trafficking of human bradykinin receptors: arrestin-and dynamin-independent sequestration of the B2 receptor and bradykinin in HEK293 cells. *Biochemical Journal* **355**, 741-750 (2001).

37 Haasemann, M., Cartaud, J., Müller-Esterl, W. & Dunia, I. Agonist-induced redistribution of bradykinin B 2 receptor in caveolae. *Journal of cell science* **111**, 917-928 (1998).

38 Blaukat, A. *et al.* Determination of bradykinin B2 receptor in vivo phosphorylation sites and their role in receptor function. *Journal of Biological Chemistry* **276**, 40431-40440 (2001).

39 Pizard, A., Blaukat, A., Muller-Esterl, W., Alhenc-Gelas, F. & Rajerison, R. M. Bradykinin-induced internalization of the human B2receptor requires phosphorylation of three serine and two threonine residues at its carboxyl tail. *Journal of Biological Chemistry* **274**, 12738-12747 (1999).

40 Janetzko, J. *et al.* Membrane phosphoinositides regulate GPCR-β-arrestin complex assembly and dynamics. *Cell* **185**, 4560-4573. e4519 (2022).

41 Fried, S. D. *et al.* Membrane curvature revisited—the archetype of rhodopsin studied by time-resolved electronic spectroscopy. *Biophysical journal* **120**, 440-452 (2021).

42 Bondar, A. *et al.* Quantitative linear dichroism imaging of molecular processes in living cells made simple by open software tools. *Communications Biology* **4**, 1-12 (2021).

43 Khoroshyy, P., Martinez-Seara, H., Myšková, J. & Lazar, J. Dynamics of transition dipole moment orientation in representative fluorescent proteins. *Physical Chemistry Chemical Physics* **25**, 22117-22123 (2023).

44 Kampmann, M., Atkinson, C. E., Mattheyses, A. L. & Simon, S. M. Mapping the orientation of nuclear pore proteins in living cells with polarized fluorescence microscopy. *Nature structural & molecular biology* **18**, 643-649 (2011).

45 Abrahamsson, S. *et al.* MultiFocus Polarization Microscope (MF-PolScope) for 3D polarization imaging of up to 25 focal planes simultaneously. *Optics express* **23**, 7734-7754 (2015).

46 Liu, T. *et al.* Deep learning-based holographic polarization microscopy. *ACS photonics* **7**, 3023-3034 (2020).

47 Chen, L. *et al.* Advances of super-resolution fluorescence polarization microscopy and its applications in life sciences. *Computational and Structural Biotechnology Journal* **18**, 2209-2216 (2020).

48 Dean, W. F., Nawara, T. J., Albert, R. M. & Mattheyses, A. OOPS: Object-Oriented Polarization Software for analysis of fluorescence polarization microscopy images. *bioRxiv*, 2023.2012. 2005.570241 (2023).

49 Bruggeman, E. *et al.* POLCAM: Instant molecular orientation microscopy for the life sciences. *bioRxiv*, 2023.2002. 2007.527479 (2023).

50 Keikhosravi, A. *et al.* Quantification of collagen organization in histopathology samples using liquid crystal based polarization microscopy. *Biomedical optics express* **8**, 4243-4256 (2017).

51 Zhanghao, K. *et al.* Super-resolution imaging of fluorescent dipoles via polarized structured illumination microscopy. *Nature Communications* **10**, 4694 (2019).